A Generation Mechanism for the Polar Cap Boundary Layer Broadband Plasma Waves

G. S. Lakhina [1] and B.T. Tsurutani
Jet Propulsion Laboratory, California Institute of Technology, Pasadena, Cal., USA

Short title: GENERATION MECHANISM OF BROADBAND PLASMA WAVES

Abstract.

Recent POLAR observations indicate the presence of broadband plasma waves in the frequency range of $\sim 10^1$ Hz to about 10^4 Hz on magnetic field lines mapping into the polar cap boundary layer, at altitudes of about 6 to 8 R_E (where R_E is the Earth radius). These waves are quite similar to the broadband plasma waves observed in the low latitude boundary layer, and they appear to be a mixture of electromagnetic and electrostatic modes. A linear theory for the generation of these waves is developed. The theory is fully electromagnetic and takes into account the free energy available due to the presence of field-aligned currents, and gradients in the currents, plasma densities and magnetic fields. A generalized dispersion relation for the coupled lower hybrid, whistler, and current convective modes is obtained. It is found that the presence of density gradients, the current convective modes develop a finite real frequency, but at the same time their growth rates are reduced. On the other hand, sharp density gradients can lead to the excitation of a lower hybrid drift instability when the hot ions are present in the boundary layer. In general the current convective and lower hybrid drift modes are coupled, and the dispersion relation has to be solved numerically. The inclusion of electromagnetic effects leads to the reduction of the growth rates.

1. Introduction

Recently, POLAR has detected broadband plasma waves in the frequency range of $\sim 10^1$ Hz to about 10^4 Hz on similar magnetic field lines as the low latitude boundary layer (LLBL) at altitudes of about 6 to 8 R_E (where R_E is the Earth radius) [*Tsurutani et al.*, 1998]. The waves appear to be a mixture of electromagnetic and electrostatic modes. The region of wave activity bounds the dayside (05 to 18 LT) polar cap fields, and thus these waves were called Polar Cap Boundary Layer (PCBL) waves [*Tsurutani et al.*, 1998]. There is a strong relationship between the presence of ionospheric and magnetosheath ions and the intense PCBL waves near the noon sector. These waves may, therefore, be responsible for ion heating/acceleration observed near the cusp region. Earlier, the broadband plasma waves have been detected within the Earth's magnetopause low latitude boundary layer (LLBL) by several spacecraft, like the ISEE-1 and -2, GEOS, and AMPTE [*Gurnett et al.*, 1979; *Tsurutani et al.*, 1981; 1989; *Anderson et al.*, 1982; *Gendrin*, 1983; *Rezeau et al.*, 1989; *Belmont et al.*, 1995; *LaBelle and Treumann*, 1988]. Similar waves have also been detected at the Jovian (magnetopause) low latitude boundary layer [*Tsurutani et al.*, 1993; 1997]. These boundary layer waves have been demonstrated to be sufficiently intense to cause cross-field diffusion of magnetosheath plasma to form the boundary layer itself at both Earth and Jupiter [*Tsurutani and Thorne*, 1982; *Tsurutani et al.*, 1997]. The cross-field diffusion of particles, energy and momentum due to the broadband plasma waves would be one form of viscous interaction between the solar wind and the magnetosphere [*Axford and Hines*, 1961; *Tsurutani and Gonzalez*, 1995].

The generation mechanism of the PCBL as well as LLBL waves is not well understood. The emissions are broadbanded with no obvious spectral peaks which could be used to identify particular plasma instabilities. Some suggested mechanisms for the LLBL waves are the electron loss cone instability driven by velocity space gradients [*Kennel and Petschek*, 1966], the lower hybrid drift instability driven essentially by

the density gradients [*Gary and Eastman*, 1979; *Huba et al.*, 1981], the velocity shear and drift instabilities [*Lakhina*, 1987; 1993; *Ganguli et al.*, 1994; *Lakhina et al.*, 1995], and a magnetic shear instability [*Zhu et al.*, 1996]. An electrostatic current convective instability [*Drake et al.*, 1994a] and a whistler instability [*Drake et al.*, 1994b; *Drake* , 1995] driven unstable by the gradient of the field-aligned currents have been proposed. However, the last two mechanisms employ cold plasma approximation, and they work best for the thin magnetopause current layers .

In this paper we present a linear theory for the generation of broadband PCBL plasma waves. The theory is fully electromagnetic and takes into account the free energy available due to the presence of field-aligned currents, and gradients in the currents, plasma densities and magnetic fields. The dispersion relation generalizes the dispersion relations for the lower hybrid and current convective instabilities. In general the current convective and lower hybrid drift modes are coupled, and the dispersion relation has to be solved numerically.

2. The Model

Let us consider the PCBL wave region to be characterized by nonuniform plasma and magnetic field. In the equilibrium state, there is a finite field-aligned current. For simplicity, we consider the currents to be carried by electrons streaming with a nonuniform velocity $\mathbf{V}_0(x)$ relative to ions. This field-aligned currents makes the magnetic field nonuniform. The equilibrium magnetic field varies along x-direction, the direction of inhomogeneity, and is directed along the z axis, i.e., $\mathbf{B}_0 = B_0(x)\,\mathbf{z}$. In the equilibrium state, the electron and ion densities are taken to be equal, i.e., $n_{0e}(x) = n_{0i}(x) = n_0(x)$ to maintain the charge neutrality. We consider the waves propagating obliquely to the ambient magnetic field in the y-z plane, i.e., the wave vector, k, can be written as $\mathbf{k} = k_z\,\mathbf{z} + k_y\,\mathbf{y}$. We shall consider the frequency range $\omega_{ci}^2 \ll \omega^2 \ll \omega_{ce}^2$, where $\omega_{ci}(\omega_{ce})$ is the ion (electron) cyclotron frequency. Under

this assumption ion response to the perturbation can be treated as unmagnetized. Electrons are treated as magnetized and their response to perturbation is taken as fully electromagnetic.

The dynamics of the plasma is governed by two fluid equations. For electron dynamics is described by the continuity and parallel momentum equations,

$$\frac{\partial n_e}{\partial t} + \nabla_\perp \cdot (n_e \mathbf{v}_{\perp e}) + \frac{\partial (n_e v_{ze})}{\partial z} = 0, \tag{1}$$

$$\frac{\partial v_{ze}}{\partial t} + \mathbf{v}_e \cdot \nabla v_{ze} = -\frac{e}{m_e} E_z - \frac{V_{te}^2}{n_e} \frac{\partial n_e}{\partial z} - \frac{e}{m_e} \mathbf{V}_{de} \times \mathbf{B} - \frac{e}{m_e} \mathbf{V}_{pe} \times \mathbf{B}, \tag{2}$$

where

$$\mathbf{v}_{\perp e} \approx \mathbf{v}_E + \mathbf{V}_{de} + \mathbf{V}_{pe}, \tag{3}$$

is the perpendicular components of the electron fluid velocity, $\mathbf{v}_e$. Here $\mathbf{v}_E = (1/B_0)\mathbf{E} \times \mathbf{z}$, $\mathbf{V}_{de} = -(V_{te}^2/\omega_{ce})\mathbf{z} \times \nabla \ln n_e$, $\mathbf{V}_{pe} = (1/B_0\omega_{ce})(\partial \mathbf{E}_\perp/\partial t + \mathbf{v}_e \cdot \nabla \mathbf{E}_\perp)$ are, respectively, the $\mathbf{E} \times \mathbf{B}$ drift, the density gradient drift and the polarization drift. Further, $\omega_{ce} = (e\,B_0/m_e)$ is the electron cyclotron frequency, n_e is the electron number density, m_e is the electron mass, T_e is the electron temperature, $V_{te} = (T_e/m_e)^{1/2}$ is the electron thermal velocity, and $\mathbf{E}_\perp$ is the perpendicular (to $B_0\,\mathbf{z}$) component of the wave electric field vector, and $\mathbf{B} = \mathbf{B_0} + \mathbf{B_1}$ is the total magnetic field, with $\mathbf{B_1}$ being the wave magnetic field. The ion dynamics is governed by

$$\frac{\partial n_i}{\partial t} + \nabla_\perp \cdot (n_i \mathbf{v}_{\perp i}) + \frac{\partial (n_i v_{zi})}{\partial z} = 0, \tag{4}$$

$$\frac{\partial \mathbf{v}_i}{\partial t} + \mathbf{v}_i \cdot \nabla \mathbf{v}_i = -\frac{e}{m_i} \mathbf{E} - \frac{V_{ti}^2}{n_i} \nabla n_i, \tag{5}$$

where the i subscript denote the corresponding ion quantities.

Equations (1) to (5) along with the Maxwell's equations,

$$\frac{\partial \mathbf{B}}{\partial t} = -\nabla \times \mathbf{E}, \tag{6}$$

$$\nabla \times \mathbf{B} = \mu_0 \mathbf{J} + \mu_0 \epsilon_0 \frac{\partial \mathbf{E}}{\partial t}, \tag{7}$$

and

$$\nabla \cdot \mathbf{E} = \frac{e(n_i - n_e)}{\epsilon_0};\ \nabla \cdot \mathbf{B} = 0, \tag{8}$$

where $\mathbf{J}$ is the current density, form a basic set of equations on which the linear stability analysis would be performed. We write a quantity $g = g_0 + g_1$, where $g_1(<< g_0)$ is the perturbation, and take the perturbations in all the quantities to be of the form $g_1 \sim g_1 \exp[ik_z z + ik_y y - i\omega t]$. The dispersion relation is obtained from the linearized set of equations (1) to (8) under the local approximation which assumes the wave wavelengths to be much shorter than the inhomogeneity (e.g. in density, magnetic field, or velocity) scale length.

3. The Dispersion Relation

From the linearized form of (2), (4) and (5), we get,

$$v_{1xe} = \frac{-i}{(\omega - k_z V_0)}\left[v_{xe}\frac{dV_0}{dx} + \frac{eE_z}{m_e} + ik_z V_{te}^2 N_{1e} + V_{te}^2 \kappa_n \frac{B_{1x}}{B_0}\right], \tag{9}$$

$$N_{1i} = \frac{ie\mathbf{k}\cdot\mathbf{E}}{m_i f_1^2}, \tag{10}$$

$$\mathbf{v}_{1i} = \frac{i}{(\omega - k_y V_{d0})}\left[\frac{e\mathbf{E}}{m_i} - i\mathbf{k}V_{ti}^2 N_{1i}\right], \tag{11}$$

where $f_1^2 = [(\omega - k_y V_{d0})^2 - k^2 V_{ti}^2]$.

In the above equations, $N_{1j} = n_{1j}/n_0$ is the normalized density perturbations of the jth fluid, $\kappa_n = d\ln n_0/dx$ is the inverse of equilibrium density gradient, $\kappa_B = d\ln B_0/dx$ is the inverse of the ambient magnetic field gradient. Further, we have taken into account the cross-field ion drift relative to the electrons, V_{d0}, which can arise due to the density gradients, or due to some other processes. For the case of density gradients, the relative cross-field drift velocity is simply given by $\mathbf{V}_{d0} = [\kappa_n V_{ti}^2(1 + T_e/T_i)/\omega_{ci}]\,\mathbf{y}$. Here, ω_{cj} represents the cyclotron frequency of the jth species (with $j = e$ for the electrons and $j = i$ for the ions). On substituting for $\mathbf{v}_{1\perp e}$ and v_{1xe} from (3) and (9), respectively,

in linearized form of (1), we get

$$N_{1e} = \frac{i(\omega - k_z V_0)}{f_2^2}\left[-\frac{E_y(\kappa_n - \kappa_B)}{B_0} + \frac{E_y k_y(\omega - k_z V_0)}{B_0\omega_{ce}} + \right.$$
$$+\frac{iE_x(2\kappa_B - \kappa_n)(\omega - k_z V_0)}{B_0\omega_{ce}} - \frac{k_z}{(\omega - k_z V_0)}\left\{\frac{eE_z}{m_e} + \right.$$
$$\left.\left.+\frac{dV_0}{dx}\left(\frac{E_y}{B_0} + \frac{iE_x(\omega - k_z V_0)}{B_0\omega_{ce}}\right) + V_{te}^2\kappa_n\frac{B_{1x}}{B_0}\right\} - \frac{i\omega B_{1z}}{B_0}\right], \qquad (12)$$

where $f_2^2 = [(\omega - k_z V_0)^2 - k_z^2 V_{te}^2(1 + \frac{k_y}{k_z\omega_{ce}}\frac{dV_0}{dx})]$.

On taking the curl of (7) and then considering the z component of the resulting equation, we get

$$\frac{B_{1z}}{B_0} = \frac{\omega_{pe}^2}{c^2k^2\omega_{ce}}\left[k_y\left(\frac{\omega_{ci}}{\omega - k_y V_{d0}} - \frac{\omega - k_z V_0}{\omega_{ce}}\right)\frac{E_x}{B_0} + \right.$$
$$\left.+ik_y\left(1 + \frac{F_1\omega_{ci}}{f_1^2}\right)\frac{E_y}{B_0} + \frac{ik_z F_1\omega_{ci}}{f_1^2}\frac{E_z}{B_0}\right], \qquad (13)$$

where

$$F_1 = -\frac{k_y^2 V_{te}^2}{\omega_{ce}} + \frac{dV_{d0}}{dx}, \qquad (14)$$

and $\omega_{pe} = (n_0e^2/\epsilon_0 m_e)^{1/2}$ is the electron plasma frequency, and $c = (\mu_0\epsilon_0)^{-1/2}$ is the speed of light. In deriving (13), we have taken $\omega^2 \ll c^2k^2$. On substituting for N_{1i} from (10), N_{1e} from (12), B_{1x} from linearized form of (6), and B_{1z} from (13) into the linearized version of the Poisson's equation (8), we get

$$a_{11}E_x + a_{12}E_y + a_{13}E_z = 0, \qquad (15)$$

where

$$a_{11} = \frac{i\omega_{pe}^2(\omega - k_z V_0)}{\omega_{ce}^2 f_2^2}\left[k_z\frac{dV_0}{dx} + k_y\omega\frac{\omega_{pe}^2}{c^2k^2}\left(\frac{\omega_{ci}}{\omega - k_y V_{d0}} - \frac{\omega - k_z V_0}{\omega_{ce}}\right)\right]$$
$$a_{12} = -k_y\left(1 - \frac{\omega_{pi}^2}{f_1^2}\right) - \frac{\omega_{pe}^2(\omega - k_z V_0)}{f_2^2}\left[-\frac{(\kappa_n - \kappa_B)}{\omega_{ce}} + \frac{k_y(\omega - k_z V_0)}{\omega_{ce}^2} - \right.$$
$$\left.-\frac{k_z}{(\omega - k_z V_0)}\left(\frac{1}{\omega_{ce}}\frac{dV_0}{dx} - \frac{k_z\kappa_n V_{te}^2}{\omega\omega_{ce}}\right) + \frac{\omega_{pe}^2}{c^2k^2}\frac{k_y\omega}{\omega_{ce}^2}(1 + \frac{\omega_{ci}F_1}{f_1^2})\right]$$
$$a_{13} = -k_z\left(1 - \frac{\omega_{pi}^2}{f_1^2}\right) + \frac{\omega_{pe}^2 k_z}{f_2^2}\left[\left(1 + \frac{k_y\kappa_n V_{te}^2}{\omega\omega_{ce}}\right) - \frac{\omega_{pe}^2}{c^2k^2}\frac{\omega(\omega - k_z V_0)}{\omega_{ce}^2}\frac{\omega_{ci}F_1}{f_1^2}\right] \qquad (16)$$

On taking the z component of (7), and making use of (9)-(12), we can obtain an expression for $(\mathbf{k}\times\mathbf{B_1})_z$. Equating this with the $(\mathbf{k}\times\mathbf{B_1})_z$ obtained by taking a curl of (6) and then considering the z component, we arrive at,

$$a_{21}E_x + a_{22}E_y + a_{23}E_z = 0, \tag{17}$$

where

$$\begin{aligned}
a_{21} &= -\frac{\omega_{pe}^2}{c^2}\left[\frac{i}{\omega_{ce}^2}\frac{dV_0}{dx} - \frac{(\omega - k_zV_0)}{f_2^2}\left\{\frac{i\omega(2\kappa_B-\kappa_n)}{\omega_{ce}^2} - \right.\right. \\
&\left.\left. -\frac{ik_z}{\omega_{ce}^2}\frac{dV_0}{dx}\right\}\cdot\left\{\frac{k_yV_{te}^2}{(\omega-k_zV_0)\omega_{ce}}\frac{dV_0}{dx} + \frac{k_zV_{te}^2}{(\omega-k_zV_0)} + V_0\right\}\right] \\
a_{22} &= \frac{k_zk_y}{\omega} - \frac{\omega_{pe}^2}{c^2}\left[\frac{m_e}{m_i}\frac{k_zk_yV_{ti}^2}{(\omega-k_yV_{d0})f_1^2} + \frac{1}{(\omega-k_zV_0)}\left(\frac{1}{\omega_{ce}}\frac{dV_0}{dx} - \frac{k_z\kappa_nV_{te}^2}{\omega\omega_{ce}}\right) - \right. \\
&-\frac{1}{f_2^2}\left\{-\frac{(\kappa_n-\kappa_B)}{\omega_{ce}} + \frac{(\omega-k_zV_0)k_y}{\omega_{ce}^2} - \frac{k_z}{(\omega-k_zV_0)}\left(\frac{1}{\omega_{ce}}\frac{dV_0}{dx} - \frac{k_z\kappa_nV_{te}^2}{\omega\omega_{ce}}\right)\right\} \\
&\left.\cdot\left\{\frac{k_yV_{te}^2}{\omega_{ce}}\frac{dV_0}{dx} + k_zV_{te}^2 + V_0(\omega-k_zV_0)\right\}\right] \\
a_{23} &= -\frac{k_y^2}{\omega} + \frac{\omega}{c^2} - \frac{\omega_{pe}^2}{c^2}\left[\frac{m_e}{m_i}\frac{1}{(\omega-k_yV_{d0})}\left(1+\frac{k_z^2V_{ti}^2}{f_1^2}\right) + \frac{1}{(\omega-k_zV_0)}\left(1+\frac{k_y\kappa_nV_{te}^2}{\omega\omega_{ce}}\right) + \right. \\
&\left. + \frac{k_z}{f_2^2}\left(1+\frac{k_y\kappa_nV_{te}^2}{\omega\omega_{ce}}\right)\cdot\left\{\frac{k_yV_{te}^2}{(\omega-k_zV_0)\omega_{ce}}\frac{dV_0}{dx} + \frac{k_zV_{te}^2}{(\omega-k_zV_0)} + V_0\right\}\right]
\end{aligned} \tag{18}$$

Considering the z component of (6), we get

$$\frac{B_{1z}}{B_0} = -\frac{k_yE_x}{\omega B_0}. \tag{19}$$

On equating right hand sides of (13) and (19), we arrive at,

$$a_{31}E_x + a_{32}E_y + a_{33}E_z = 0, \tag{20}$$

where

$$\begin{aligned}
a_{31} &= \frac{k_y}{\omega}\left[1 + \frac{\omega_{pe}^2\omega}{c^2k^2\omega_{ce}}\left(\frac{\omega_{ci}}{\omega-k_yV_{d0}} - \frac{\omega-k_zV_0}{\omega_{ce}}\right)\right], \\
a_{32} &= \frac{i\,k_y\omega_{pe}^2}{c^2k^2\omega_{ce}}\left(1+\frac{F_1\omega_{ci}}{f_1^2}\right), \\
a_{33} &= \frac{ik_z\,F_1\omega_{ci}}{f_1^2}\frac{\omega_{pe}^2}{c^2k^2\omega_{ce}}.
\end{aligned} \tag{21}$$

Combining (15), (17), and (20), we get the dispersion relation,

$$a_{11}(a_{22}a_{33} - a_{32}a_{23}) - a_{12}(a_{21}a_{33} - a_{23}a_{31}) + a_{13}(a_{21}a_{32} - a_{22}a_{31}) = 0 \qquad (22)$$

After a considerable algebra, and neglecting the terms $\sim m_e/m_i$, (22) can be simplified to,

$$\begin{aligned}
&\left[1 - \frac{\omega_{pi}^2}{f_1^2} + \frac{\omega_{pe}^2(\omega - k_z V_0)}{f_2^2 \omega_{ce}} \left\{ - \frac{(\kappa_n - \kappa_B)}{k_y} + \frac{(\omega - k_z V_0)}{\omega_{ce}} - \right.\right. \\
&\left.\left. - \frac{k_z}{k_y(\omega - k_z V_0)} \left(\frac{dV_0}{dx} - \frac{k_z \kappa_n V_{te}^2}{\omega} \right) + \frac{\omega_{pe}^2}{c^2 k^2} \frac{\omega}{\omega_{ce}} \left(1 + \frac{\omega_{ci} F_1}{f_1^2} \right) \right\} \right] \cdot \\
&\cdot \left[1 + \frac{\omega_{pe}^2 \omega^2}{c^2 k_y^2 f_2^2} \left\{ 1 + \frac{k_y \kappa_n V_{te}^2}{\omega \omega_{ce}} + \frac{\frac{\omega_{pe}^2}{c^2 k^2} \frac{\omega(\omega - k_z V_0)}{\omega_{ce}^2} \frac{1}{\omega_{ce}} \frac{dV_0}{dx} \frac{k_z}{k_y} \frac{\omega_{ci} F_1}{f_1^2}}{\left\{ 1 + \frac{\omega_{pe}^2 \omega}{c^2 k^2 \omega_{ce}} \left(\frac{\omega_{ci}}{\omega - k_y V_{d0}} - \frac{\omega - k_z V_0}{\omega_{ce}} \right) \right\}} \right\} \right] + \\
&+ \left[\frac{k_z^2}{k_y^2} - \frac{\omega_{pe}^2}{c^2 k_y^2} \frac{\omega}{(\omega - k_z V_0)} \left\{ \frac{1}{\omega_{ce}} \frac{dV_0}{dx} \frac{k_z}{k_y} - \frac{k_z^2 \kappa_n V_{te}^2}{k_y \omega \omega_{ce}} - \right.\right. \\
&\left.\left. - \frac{(\omega - k_z V_0)}{f_2^2 \omega_{ce}} \left(- \frac{(\kappa_n - \kappa_B)}{k_y} + \frac{(\omega - k_z V_0)}{\omega_{ce}} - \frac{k_z \omega_{ce}}{k_y(\omega - k_z V_0)} \cdot \right.\right.\right. \\
&\left.\left.\left. \cdot \left(\frac{1}{\omega_{ce}} \frac{dV_0}{dx} - \frac{k_z \kappa_n V_{te}^2}{\omega \omega_{ce}} \right) \right) \cdot \left(\frac{k_z k_y V_{te}^2}{\omega_{ce}} \frac{dV_0}{dx} + k_z^2 V_{te}^2 + k_z V_0(\omega - k_z V_0) \right) \right\} \right] \cdot \\
&\cdot \left[1 - \frac{\omega_{pi}^2}{f_1^2} + \frac{\omega_{pe}^2(\omega - k_z V_0)}{f_2^2 \omega_{ce}} \left\{ - \frac{\omega_{ce}}{(\omega - k_z V_0)} \left(1 + \frac{k_y \kappa_n V_{te}^2}{\omega \omega_{ce}} \right) + \frac{\omega_{pe}^2}{c^2 k^2} \frac{\omega_{ci}}{\omega_{ce}} \frac{\omega F_1}{f_1^2} \right\} - \right. \\
&\left. - \frac{\omega_{pe}^4 \omega(\omega - k_z V_0)}{c^2 k^2 \omega_{ce}^2 f_2^2} \frac{\omega_{ci} F_1}{f_1^2} \frac{\left(\frac{1}{\omega_{ce}} \frac{dV_0}{dx} \frac{k_z}{k_y} + \frac{\omega_{pe}^2 \omega}{c^2 k^2 \omega_{ce}} \left(\frac{\omega_{ci}}{\omega - k_y V_{d0}} - \frac{\omega - k_z V_0}{\omega_{ce}} \right) \right)}{\left\{ 1 + \frac{\omega_{pe}^2 \omega}{c^2 k^2 \omega_{ce}} \left(\frac{\omega_{ci}}{\omega - k_y V_{d0}} - \frac{\omega - k_z V_0}{\omega_{ce}} \right) \right\}} \right] - \\
&- \frac{\omega_{pe}^4 \omega(\omega - k_z V_0)}{c^2 k^2 \omega_{ce}^2 f_2^2} \cdot \frac{\left(1 + \frac{\omega_{ci} F_1}{f_1^2} \right)}{\left\{ 1 + \frac{\omega_{pe}^2 \omega}{c^2 k^2 \omega_{ce}} \left(\frac{\omega_{ci}}{\omega - k_y V_{d0}} - \frac{\omega - k_z V_0}{\omega_{ce}} \right) \right\}} \cdot \left[\frac{\omega^2}{c^2 k_y^2} \frac{1}{\omega_{ce}} \frac{dV_0}{dx} \frac{k_z}{k_y} \left\{ 1 - \frac{\omega_{pi}^2}{f_1^2} + \right.\right. \\
&\left.\left. + \frac{\omega_{pe}^2(\omega - k_z V_0)}{f_2^2 \omega_{ce}} \cdot \left\{ - \frac{\omega_{ce}}{(\omega - k_z V_0)} \left(1 + \frac{k_y \kappa_n V_{te}^2}{\omega \omega_{ce}} \right) + \frac{\omega_{pe}^2}{c^2 k^2} \frac{\omega_{ci}}{\omega_{ce}} \frac{\omega F_1}{f_1^2} \right\} \right\} + \right. \\
&\left. + \left\{ \frac{1}{\omega_{ce}} \frac{dV_0}{dx} \frac{k_z}{k_y} + \frac{\omega_{pe}^2 \omega}{c^2 k^2 \omega_{ce}} \cdot \left(\frac{\omega_{ci}}{\omega - k_y V_{d0}} - \frac{\omega - k_z V_0}{\omega_{ce}} \right) \right\} \cdot \right. \\
&\left. \cdot \left\{ 1 + \frac{\omega_{pe}^2}{c^2 k_y^2} \frac{\omega^2}{f_2^2} \left(1 + \frac{k_y \kappa_n V_{te}^2}{\omega \omega_{ce}} \right) \right\} \right] = 0. \qquad (23)
\end{aligned}$$

3.1. Special Case: Electrostatic Modes

Under the limit of $R \equiv \omega_{pe}^2/c^2k^2 \to 0$, (23) is greatly simplified to,

$$1 - \frac{\omega_{pi}^2}{f_1^2} - \frac{\omega_{pe}^2 k_z^2}{f_2^2 k^2} + \frac{k_y^2}{k^2} \frac{\omega_{pe}^2(\omega - k_z V_0)^2}{f_2^2 \omega_{ce}^2} - \frac{k_y(\kappa_n - \kappa_B)}{k^2} \frac{\omega_{pe}^2(\omega - k_z V_0)}{f_2^2 \omega_{ce}} - \frac{k_z k_y}{k^2} \frac{1}{\omega_{ce}} \frac{dV_0}{dx} \frac{\omega_{pe}^2}{f_2^2} = 0. \qquad (24)$$

3.1.1. Current convective modes. For the case of cold plasma, and $\omega^2 \gg k_z^2 V_0^2$, (24) reduces to

$$1 + \frac{k_y^2}{k^2}\frac{\omega_{pe}^2}{\omega_{ce}^2} - \frac{k_y(\kappa_n - \kappa_B)}{k^2}\frac{\omega_{pe}^2}{\omega\omega_{ce}} - \frac{\omega_{pi}^2}{\omega^2} - \frac{k_z^2}{k^2}\frac{\omega_{pe}^2}{\omega^2}\left(1 + \frac{k_y}{k_z}\frac{1}{\omega_{ce}}\frac{dV_0}{dx}\right) = 0, \qquad (25)$$

which is identical to that of *Ganguli et al.* [1994] and *Drake et al.*[1994a] in the limit of uniform plasma (i.e., $\kappa_n = \kappa_B = 0$) and unmagnetized ions. For the case of uniform plasma and magnetic fields, (25) yields a solution for the current convective mode,

$$\omega^2 = \frac{k_z^2}{k^2}\frac{\omega_{pe}^2}{\left(1 + \frac{k_y^2}{k^2}\frac{\omega_{pe}^2}{\omega_{ce}^2}\right)}\left[\frac{k_y}{k_z}S + \left(1 + \frac{k^2}{k_z^2}\frac{m_e}{m_i}\right)\right], \qquad (26)$$

where $S \equiv \frac{1}{\omega_{ce}}\frac{dV_0}{dx}$ is the velocity shear. Clearly, there is a possibility of the unstable modes for the case when $(k_y/k_z)S < 0$. For simplicity we shall consider the velocity shear to be positive, i.e., $S > 0$. Then, for $k_z/k_y < 0$, the current convective modes could become unstable provided the velocity shear satisfies the following inequality,

$$S > \left|\frac{k_z}{k_y}\right|\left(1 + \frac{k^2}{k_z^2}\frac{m_e}{m_i}\right). \qquad (27)$$

From (27), it is clear that minimum velocity shear, S_{min} required to excite the current convective instability is $S_{min} = 2\sqrt{m_e/m_i}$ occurring at a certain critical wave propagation angle of $(k_z/k_y)_{cr} \approx -\sqrt{m_e/m_i}$. The growth rate of the mode at the critical angle of propagation (i.e., at $(k_z/k_y) = (k_z/k_y)_{cr}$) would be

$$\gamma = \left(\frac{m_i}{m_e}\right)^{\frac{1}{4}}\omega_{lh}(S - S_{min})^{\frac{1}{2}}, \qquad (28)$$

where

$$\omega_{lh} = \frac{\omega_{pi}}{\left(1 + \frac{\omega_{pe}^2}{\omega_{ce}^2}\right)^{1/2}} \qquad (29)$$

is the lower hybrid frequency.

For the case of nonuniform plasma, (25) predict unstable roots provided the velocity shear exceeds a threshold value,

$$S > S_0 = \left|\frac{k_z}{k_y}\right|\left[1 + \frac{k^2}{k_z^2}\frac{m_e}{m_i} + \frac{k_y^2(\kappa_n - \kappa_B)^2}{4k_z^2k^2\omega_{ce}^2}\frac{\omega_{pe}^2}{\left(1 + \frac{k_y^2}{k^2}\frac{\omega_{pe}^2}{\omega_{ce}^2}\right)}\right]. \qquad (30)$$

The minimum value of S_0 is found to be $S_{th} = 2\sqrt{m_e/m_i}\sqrt{\alpha}$, and it occurs at a critical value of wave propagation angle, $(k_z/k_y)_{cr} \approx -\sqrt{m_e/m_i}\sqrt{\alpha}$, where

$$\alpha = 1 + \frac{(\kappa_n - \kappa_B)^2}{4k_y^2}\frac{m_i^2}{m_e^2}\frac{\omega_{lh}^2}{\omega_{ce}^2} \tag{31}$$

Further, at the critical angle of propagation, the real frequency, ω_r, and the growth rate, γ, of the mode are given by,

$$\begin{aligned} \omega_r &= \frac{(\kappa_n - \kappa_B)}{2k_y\omega_{ci}}\omega_{lh}^2, \\ \gamma &= \left(\frac{m_i}{m_e}\right)^{\frac{1}{4}} \alpha^{\frac{1}{4}}\omega_{lh}(S - S_{th})^{\frac{1}{2}}. \end{aligned} \tag{32}$$

Since $S_{th} \geq S_{min}$, it is clear that the density and magnetic field gradients tend to stabilize the current convective modes. Further, in the presence of density and magnetic field gradients, the current connective modes develop real frequencies as seen from (32).

In Figure 1 we have shown some results for the electrostatic current convective modes in a cold plasma obtained by solving (25) numerically. For the case of uniform plasma, the current convective instability is purely growing as expected from (26) and (28) (cf. curves 1 and 2). The instability occurs only for negative values of (k_z/k_y). The growth rate is reduced by a decrease in the value of (k_z/k_y). For the case of inhomogeneous plasma, the modes develop a real frequency which increases with an increase in $(\kappa_n - \kappa_B)/k_y)$, but the growth rates are reduced when $(\kappa_n - \kappa_B)/k_y)$ increases (cf. curves 3,4, and 5). At the same time increasingly higher values of S are needed to excite the instability when the parameter $(\kappa_n - \kappa_B)/k_y)$, increases. Hence the density and magnetic field gradients have a stabilizing effect on the current convective instability.

3.2. Special Case: Electromagnetic Modes

Once again restricting to a cold plasma and considering system $\omega^2 \gg k_z^2 V_0^2,\ k_y^2 V_{d0}^2$, $\omega^2 \ll \omega_{pe}^2$, and neglecting terms $\sim m_e/m_i$ as compared to 1, (23) can be simplified to

$$\Delta - \frac{(\kappa_n - \kappa_B)}{k_y}\frac{\omega_{pe}^2}{\omega\omega_{ce}} - \frac{\omega_{pi}^2}{\omega^2} - \frac{k_z^2}{k^2}\frac{\omega_{pe}^2}{\omega^2(1+R)}\left(1 + \frac{k_y}{k_z}S\right) = 0, \tag{33}$$

where,

$$\Delta = 1 + \frac{\omega_{pe}^2}{\omega_{ce}^2}\left[(1+R) - \frac{RS}{(1+R)}\frac{k_z}{k_y}\right]. \tag{34}$$

When the velocity shear is neglected, and appropriate limits are considered, (33) reduces to the dispersion relation obtained by *Lakhina and Sen* [1973] and *Winske and Omidi* [1995].

3.2.1. Whistler mode instabilities. In the absence of density and magnetic field gradients, i.e., $\kappa_n = \kappa_B = 0$, (33) yields

$$\omega^2 = \frac{k_z^2}{k^2}\frac{\omega_{pe}^2}{\Delta(1+R)}\left[\frac{k_y}{k_z}S + \left(1 + \frac{k^2}{k_z^2}\frac{m_e}{m_i}(1+R)\right)\right], \tag{35}$$

which for $R = 0$ goes over to (26). On taking $\omega_{pe}^2/\omega_{ce}^2 \gg 1$, and $R \gg 1$ in (35), we get

$$\omega = \frac{c^2k^2}{\omega_{pe}^2}\omega_{ce}\cos\theta\left[1 + \frac{k^2}{k_z^2}\frac{m_e}{m_i}R + \frac{k_y}{k_z}S\right]^{\frac{1}{2}}, \tag{36}$$

where $\cos\theta = k_z/k$ is the angle of propagation with respect to the ambient magnetic field. On neglecting the ion dynamics (i.e., the second term inside the bracket on the right hand side), and the velocity shear effects (i.e., putting $S = 0$), (36) becomes identical to the dispersion relation for the oblique whistler waves [*Stix*, 1992; *Drake*, 1995]. Equation (36) predicts a whistler mode instability provided the velocity shear exceeds a certain value,

$$S > \left|\frac{k_z}{k_y}\right|\left(1 + \frac{k^2}{k_z^2}\frac{m_e}{m_i}R\right). \tag{37}$$

For $m_eR/m_i \ll 1$, the minimum value of the whisler mode instability threshold is simply $S_{wm} = 2\sqrt{m_e/m_i}\sqrt{R}$, and it occurs at the wave propagation angle corresponding to

$(k_z/k_y)_{cr} \approx -\sqrt{m_e/m_i}\sqrt{R}$. The growth rate, at the critical angle of propagation is given by

$$\gamma = \left(\frac{m_i}{m_e}\right)^{\frac{1}{4}} \frac{(S - S_{wm})^{\frac{1}{2}}}{R^{\frac{3}{4}}} \omega_{ce}. \tag{38}$$

For the case of nonuniform plasmas, i.e., $\kappa_n \neq 0$, $\kappa_B \neq 0$, (33) predicts an unstable mode provided

$$S > S_1 = \left|\frac{k_z}{k_y}\right| \left[1 + \frac{k^2}{k_z^2}\frac{m_e}{m_i} R\,\alpha_1\right], \tag{39}$$

where

$$\alpha_1 = 1 + \frac{(\kappa_n - \kappa_B)^2}{4k_y^2 R}\frac{m_i}{m_e} \tag{40}$$

For $m_e R/m_i \ll 1$, the minimum value of the velocity shear for exciting the whistler mode instability is simply $S^* = 2\sqrt{m_e/m_i}\sqrt{R\,\alpha_1}$, and it occurs at the wave propagation angle corresponding to $(k_z/k_y)_{cr} \approx -\sqrt{m_e/m_i}\sqrt{R\,\alpha_1}$. At the critical angle of propagation the real frequency and and the growth rate of the unstable modes are given by

$$\begin{aligned} \omega_r &= \frac{(\kappa_n - \kappa_B)}{2k_y R}\omega_{ce}, \\ \gamma &= \left(\frac{m_i}{m_e}\right)^{\frac{1}{4}} \frac{\alpha_1^{\frac{1}{4}}}{R^{\frac{3}{4}}}(S - S^*)^{\frac{1}{2}}\,\omega_{ce}. \end{aligned} \tag{41}$$

On comparing S_{wm} and S^*, it is clear that velocity shear threshold for the excitation of whistler instability is higher in the presence of density and magnetic field gradients.

In Figure 2.we have shown some results for the whistler mode instability in a cold plasma obtained by solving (33). It is seen that the growth rates are increased by an increase of velocity shear, S, but are reduced by an increase of R for both the cases of uniform plasma (cf. curves 1-3) and nonuniform plasma (cf. curves 4 and 5). This is in agreement with the analytical solutions given by (38) and (41) respectively for the uniform and nonuniform plasma case. The instability is purely growing for the uniform plasma case, but it has a finite real frequency for the nonuniform case (cf curve 4 and 5 in the lower panel). The real frequency also decreases by an increase in R.

3.2.2. Modified two stream instability in cold plasmas. Once again we consider the case of a cold plasma, but retain the cross-field electron -ion drift in (23). Assuming $\omega^2 \gg k_z^2 V_0^2$, $\omega^2 \ll \omega_{pe}^2$, and neglecting terms $\sim m_e/m_i$ as compared to 1, (23) can be reduced to

$$\Delta - \frac{(\kappa_n - \kappa_B)}{k_y}\frac{\omega_{pe}^2}{\omega\omega_{ce}} - \frac{\omega_{pi}^2}{(\omega - k_y V_{d0})^2} - \frac{k_z^2}{k^2}\frac{\omega_{pe}^2}{\omega^2(1+R)}\left(1 + \frac{k_y}{k_z}S\right) = 0, \qquad (42)$$

which generalizes the dispersion relations for the modified two-stream instability [*Krall and Liewer*, 1971; *Lakhina and Sen*, 1973] and current convective modes. It should, however, be noted that here the cross-field electron-ion relative drift, V_{d0}, does not arise due to the density gradient as the plasma is considered to be cold, rather it is being maintained by some other external means, e.g., electric field pulses, or monoenergetic ion fluxes across the magnetic field.

Figure 3 shows some results for the unstable modes obtained by the numerical solution of (42) for the situation where the current convective modes are stable. The curves 1 -3 are for the uniform plasma with velocity shear. Both the growth rate and the real frequency decrease by an increase of R. Comparing the curves 1,4 and 5, we notice that the effect of the velocity shear is stabilizing for negative value of k_z/k_y and destabilizing for positive values of k_z/k_y. An increase in $(\kappa_n - \kappa_B)/k_y$ leads to higher growth rates as well as real frequencies of the excited modes (cf. curve 1, 6 and 7).

4. Numerical Results

4.1. Lower hybrid drift and current convective instabilities

For the case of hot plasma, one has to solve (23) numerically as it is not amenable to any analytical solution. It is convenient to consider $a = k_y V_{ti}/\omega_{ci}$ and $\beta_i = 8\pi n_0 T_i/B_0^2$, which represent, respectively, the perpendicular wave number normailized by the ion gyroradius $\rho_i = V_{ti}/\omega_{ci}$, and the ratio of ion pressure to the magnetic field pressure, as independent parameters. Then, one can write $R = (m_i/m_e)(\beta_i/2a^2)$. Further, in

our numerical computations, we calculate the value of magnetic field gradient from the relation $\kappa_B = -\beta_i(1 + T_e/T_i)\kappa_n/2$.

Figure 4 shows the numerical solution of (23) for the case of electrostatic lower hybrid drift instability in a hot plasma (with $S = 0$, $\beta_i = 0$) where the cross-field electron-ion relative drift, V_{d0}, arises due to the density gradients. The growth rate are peaked at a certain value of $a = k_y V_{ti}/\omega_{ci}$. The peak-growth rate decreases, the real frequency increase, and the range of unstable wavenumbers shifts to higher value of a as the parameter k_z/k_y increase (cf. curves 1, 2 and 3). However, changing the sign (i.e., from negative to positive value) of k_z/k_y has no effect on these modes (not shown). An increase in κ_n/k_y leads to larger values for the growth rate and the real frequencies (cf. curves 2 and 4). Both the growth rate and the real frequency decrease by a decrease in ω_{pe}/ω_{ce} (cf curves 1 and 5). An increase in T_e/T_i does not affect the peak growth rate but shifts the unstable wavenumber region to smaller values of a. The real frequencies of the mode become some what higher by an increase of T_e/T_i (cf. curves 5 and 6).

Figure 5 shows the dispersion relation for the case of weakly coupled current convective and lower hybrid drift instabilities obtained from the numerical solution of (23). The coupling between the two modes is weak as we consider a small value of the density gradient (i.e., $\kappa_n/k_y = 0.01$) for this case. The growth rate tend to increase with increasing a. However, the growrh rates are reduced when either the parameter β_i increases (cf. curves 1, 2, and 3) or the parameter T_e/T_i decreases (cf curves 3 and 4). The real frequency of the excited modes gets decreased when the value of T_e/T_i is reduced.

Figure 6 shows the dispersion relation for the coupled lower hybrid and current convective modes in a hot plasma. For negative value of k_z/k_y (cf. curves 1, 2 and 3 for k_z/k_y =-0.1), the peak of the growth rate shifts towards lower frequencies as well as lower values of a, but becomes larger in magnitude as S increases (see the upper panel). However, the real frequencies of the excited modes are reduced when S increases (cf.

curves 1, 2, and 3 in the lower panel). For positive value of k_z/k_y (=0.1), the peak growth rates and the real frequencies are decreased when S is increased (cf. curves 1 and 4). An increase in β_i has a stabilizing effect on these modes as seen from curves 1, 5 and 6.

5. Discussion and Conclusions

When the plasma in the PCBL region can be considered as cold, our analysis predicts that it can support current convective, whistler, and modified two-stream instabilities. The minimum velocity shear for the excitation of current convective instability is $S_{min} = 2\sqrt{m_e/m_i}$ occurring at $(k_z/k_y)_{cr} \approx -\sqrt{m_e/m_i}$. The modes are purely growing, and the growth rates increase with an increase in S. On the other hand, the threshold velocity shear for the purely growing whistler instability is simply $S_{WM} = 2\sqrt{m_e/m_i}\sqrt{R}$, and it occurs at the wave propagation angle corresponding to $(k_z/k_y)_{cr} \approx -\sqrt{m_e/m_i}\sqrt{R}$. Density gradients tend to stabilize both the current convective and the whistler instabilities, at the same time these modes develop real frequencies. The effect of density gradients on the modified-two stream instability is destabilizing. The effect of velocity shear on these modes depends on the angle of propagation, i.e., it is stabilizing for $k_z/k_y < 0$ and destabilizing for $k_z/k_y > 0$.

For the case of hot plasma in the PCBL region, the lower hybrid drift and current convective instabilities are coupled. For the electrostatic case ($\beta_i = 0$) and $S = 0$, the peak growth rates are reduced by an increase in k_z/k_y and a decrease in the value of ω_{pe}/ω_{ce} . The coupled lower hybrid -current convective modes tend to be stabilized by an increase in the value of β_i. The velocity shear S can have either a destabilizing or a stabilizing effect on these modes depending on the sign of the parameter k_z/k_y .

It is interesting to note that the density gradients tend to reduce the growth rate of the velocity-shear modes (i.e., current convective and whistler instabilities discussed in sections 3.1 and 3.2). Since the density gradients provide a free energy source, normally

one would expect the density gradients to increase the growth rate of the instabilities, for example, modified two-stream and lower hybrid instabilities discussed above. However, in general, the effect of the density gradients, or any other free energy source, could be destabilizing for some modes and stabilizing for the others, depending upon the nature of the excited modes. It has been shown that density gradients tend to stabilize the Kelvin-Helmholtz instability which is driven by a velocity shear [*D'Angelo*, 1965; *Rome and Briggs*, 1972; *Catto et al.*, 1973; *Huba*, 1981]. Both the current convective and whistler modes, like the Kelvin-Helmholtz modes, are driven by a parallel velocity shear, and therefore their basic nature is expected to be similar to the latter. Physical mechanism of the velocity shear instability can be understood as follows (see Appendix A). In a uniform plasma, a perturbation electric field causes the electron to $\mathbf{E} \times \mathbf{B}$ drift along x. In the presence of velocity gradients, the convection of the electron flow v_z brings regions of different parallel flow to the same magnetic field line [*Drake et al.*, 1994a]. The resultant bunching of electrons along this magnetic field line produces an electric field which reinforces the initial perturbation, thereby producing an instability . The presence of a local density gradient would alter the nature of the bunching process. It introduces perturbations in the electron density, which in turn produce perturbations in the parallel electron velocity which are in the opposite direction to the perturbations in v_z produced by the velocity gradients. Thus, the presence of density gradients tend to debunch the electrons along $\mathbf{B}$ and reduce growth of the velocity shear modes.

From Figures 1-6, we note that the typical real frequencies generated by the instabilities considered here are in the range of 10 to 400 ω_{ci} with the parameter a lying in the range of $5 \leq a \leq 50$. For the PCBL region, typically ω_{ci} is $\sim$ 4 -5 Hz [*Russell et al.*, 1995, *Tsurutani et al.*, 1998], $T_i \sim 200$ eV, and $\beta_i \leq 0.05$. The typical ion gyroradius would be $\rho_i \approx 5.0$ km. Therefore the plasma rest frame frequencies of the excited modes would be of the order of 40 to 2000 Hz. In the satellite frame of reference, this frequency range would be broadened due to Doppler shifts and this

could explain the observed frequency range of the broadband waves. The typical perpendicular wavelengths associated with the unstable modes would be $\lambda_\perp = 2\pi/k_y \simeq$ (0.6 - 6.0) km. Since the general dispersion relation (23) describes coupled electrostatic and electromagnetic modes, the waves excited by the instabilities would have a mixture of electrostatic and electromagnetic modes, thus, naturally explaining an important characteristic of the PCBL waves.

It is worth pointing out that our model can be applied to explain the generation of the broadband waves observed in the Jovian boundary layer. Takeing typical parameters for the Jovian boundary layer as $B_0 = 5$ nT, $n_0 = 0.1$ cm^{-3}, $T_e = 3 \times 10^{5\circ}$ K, and $T_i = 5 \times 10^{5\circ}$ K (although there can be considerable variability in all of these parameters) [*Phillips et al.*, 1993; *Tsurutani et al.*, 1997], we have $\omega_{ci} = 76$ mHz, $\rho_i \approx 133$ km, $\beta_i \sim 0.06$, $T_e/T_i = 0.6$ and $\omega_{pe}/\omega_{ce} \approx 20$. Assuming that sufficiently strong density, magnetic fields or current gradients exits in the Jovian boundary layer, the results of Figures 1-6 would imply excitation of modes with frequencies of about 0.5 Hz to 30 Hz in the plasma rest frame with perpendicular wavelengths of 15 to 150 km. This agrees fairly well with the observed frequency band ($\sim 10^{-3}$ to 10^2 Hz) of the Jovian boundary layer waves. Once again the Doppler shifts could broaden the frequency range, thus further improving the agreement betwen the prediction of the theory and the observation.

The results shown in Figures 1 -6 are valid for the situations where the gradients in the field-aligned currents are more important than the field-aligned current themselves. Generally speaking, the field-aligned currents are the source of free energy and they could lead to the excitation of several electrostatic and electromagnetic modes via streaming instabilities provided they exceed the relevant instability threshold. The generalized dispersion relation (23) can deal with the situations where both the field-aligned currents and current gradient are equally important. However, the interpretation of the modes becomes much more complicated in the presence of strong field-aligned currents as several new modes could be excited. We are currently working on this, and the results

for these situations would be reported elsewhere.

We would like to point out that broadband electrostatic noise (BEN), with frequencies extending from the local lower hybrid frequency up to the local electron plasma frequency (or even above), has been observed in many regions of the magnetosphere, including the Earth's magnetotail [*Scarf et al.*, 1974; *Gurnett et al.*, 1976; *Cattell et al.*, 1986; *Gurnett and Frank*, 1977; *Matsumoto et al.*, 1994; *Kojima et al.*, 1997], the magnetosheath [*Anderson et al.*, 1982], and on cusp and auroral field lines [*Gurnett and Frank*, 1977; 1978; *Pottelette et al.*, 1990; *Dubouloz et al.*, 1991; *Ergun et al.*, 1998]. The magnetotail BEN emissions are correlated with ion and electrom beams, whereas auroral region BEN emissions are usually associated with ion conics and field-aligned electron beams. The waveform observations by the plasma wave instrument on board the GEOTAIL spacecraft have shown that BEN consists of a series of bipolar solitary pulses [*Matsumoto et al.*, 1994]. The broadness of the BEN frequency spectra arises from the solitary waveforms. A likely generation mechanism for BEN proposed by Matsumoto's group is based on the nonlinear evolution of the electron beam instabilities leading to the formation of the isolated Bernstein-Greene-Kruskal (BGK) potential structures which reproduce well the observed electrostatic solitary waveforms [*Omura et al.*, 1996; *Kojima et al.*, 1997]. Earlier, *Dubouloz et al.* [1991] have proposed a generation mechanism for auroral field line BEN in terms of electron acoustic solitons. The mechanisms discussed by *Matsumoto et al.* [1994] and *Dubouloz et al.* [1991] predict negatively charged structures whereas the Polar [*Franz et al.*, 1998] as well as FAST [*Ergun et al.*, 1998] observations indicate positively charged flowing potential structures . It is important to note that a potential structure, whether positive or negative, must inherently be a part of some nonlinear wave where the charges are trapped, otherwise it would rapidly disrupt due to the repulsive forces of the charges. Depending on the free energy available, some of the instabilities discussed in this paper could evolve nonlinearly into solitary waves, for example , whistler-type solitons. If

this happens it would naturally explain the recent observations on the waveform of the coherent structures (including the associated magnetic component ,if any) as reported by Polar[*Mozer et al.*, 1998; *Franz et al.*, 1998] and FAST [*Ergun et al.*, 1998] teams.

Appendix A: Physical Mechanism of Velocity Shear Instabilities

We give a simple physical picture of the mechanism by which a velocity shear $S = (dV_0/dX)\omega_{ce}^{-1}$ can excite instability and a density gradient $\kappa_n = d\ln n_0/dx$ can lead to stabilization. In this simple picture the magnetic filed $\mathbf{B}_0$ is taken as constant, the plasma is treated as cold, and only the electrostatic modes are considered. The basic equilibrium configuration is shown in Figure 7. The magnetic field $\mathbf{B}_0$ is in the z direction with the gradient of density, n_0' and parallel electron velocity, V_0' , in the x direction. We take $V_0' > 0$, $n_0' > 0$, and in addition treat them as constant over x distances of interest. An electrostatic perturbation field $\mathbf{E} = -\nabla\phi = -i(k_z\,\mathbf{z} + k_y\,\mathbf{y})\phi$ is applied to this system as shown in Figutre 7.

The E_y component of the perturbed electrostatic field would cause electrons to $\mathbf{E}\times\mathbf{B}$ drift with speed $v_x = -i\,k_y\phi/B_0$ along x direction. At any given $x = x_0$ region, low v_z electron from $x < x_0$ region would move upwards (towards $x = x_0$) and high v_z electrons from $x > x_0$ region move downwards provided $V_0' > 0$. The resulting variations of v_z along $\mathbf{B}_0$ would cause the electrons to bunch and enhance the original perturbations. The change in electron velocity $\delta v_z^{(1)}$ in time δt due to velocity gradient can be written as $\delta v_z^{(1)} = -v_x\,V_0'\delta t = i(k_y\phi V_0'/B_0)\delta t$.

Now in response to an E_z component of the perturbation electric field, the electrons would move along $\mathbf{B}_0$ and try to neutralize the charge. As a result, they will undergo a change in velocity $\delta v_z^{(2)} = (e\,i\,k_z\,\phi/m_e)\delta t$, in a time δt. Thus a change in v_z arises from the above two competing processes. Then, for local instability we must have

$(\delta v_z^{(1)} + \delta v_z^{(2)}) < 0$, or

$$\frac{k_y V_0'}{k_z \omega_{ce}} + 1 < 0. \tag{A1}$$

Since we have taken $V_0' > 0$, the system is unstable when $k_z/k_y < 0$, and provided

$$V_0' > \left|\frac{k_z}{k_y}\right| \omega_{ce}, \tag{A2}$$

which is quite similar with the exact condition for the current convective instability condition given by (27).

The above simple physical picture of the velocity shear instability assumes a uniform plasma. A local density gradient would alter the nature of the bunching process. In the presence of a density gradient in the x direction, the $\mathbf{E} \times \mathbf{B}$ drift of electrons introduces perturbations in the electron density $\delta n_e = -n_0' v_x \delta t$ in a time δt. Then, the electron density perturbation would be $n_e = -(k_y \phi n_0'/\omega B_0)$. Neglecting the ion density perturbations in the first approximation because of the high frequencies of the waves, the Poisson equation yields the dispersion relation

$$\omega = \frac{\kappa_n k_y \omega_{pe}^2}{k^2 \omega_{ce}}. \tag{A3}$$

Now the electron density perturbations would lead to perturbations in parallel electron velocity

$$\delta v_z^{(3)} \approx \frac{\omega \delta n_e}{k_z n_0} = \frac{i e k_z \phi}{m_e} \frac{k_y^2 \kappa_n^2 \omega_{pe}^2}{k_z^2 k^2 \omega_{ce}^2} \delta t. \tag{A4}$$

Then for the local instability, we must satisfy $(\delta v_z^{(1)} + \delta v_z^{(2)} + \delta v_z^{(3)}) < 0$, which for the case of $k_z/k_y < 0$ leads to the following condition

$$V_0' > \left|\frac{k_z}{k_y}\right| \omega_{ce} \left[1 + \frac{k_y^2}{k_z^2} \frac{\kappa_n^2}{k^2} \frac{\omega_{pe}^2}{\omega_{ce}^2}\right], \tag{A5}$$

The effect of density gradient on the velocity shear instability is always stabilizing because $\delta v_z^{(3)}$ is in the same direction as $\delta v_z^{(2)}$. For the case of hot electrons, the relevant mode frequency is $\omega \approx k_y \kappa_n V_{te}^2/\omega_{ce}$ instead of ω given by (A3). In this case also the density gradient has a stabilizing effect as seen from (A4).

The above physical picture would get modified for the general case of electromagnetic perturbations due to the Lorentz force effects.

Acknowledgments. Portions of this paper represent work done at the Jet Propulsion Laboratory, California Institute of Technology, Pasadena, under contract with the National Aeronautics and Space Administration and under subcontract with the University of Iowa. G. S. Lakhina would like to thank the National Research Council for the award of a Senior Resident Associateship at Jet Propulsion Laboratory.

References

Anderson, R. R., C. C. Harvey, M. M. Hoppe, B. T. Tsurutani, T. E. Eastman, and J. Etcheto, Plasma waves near the magnetopause, *J. Geophys. Res., 87,* 2087, 1982.

Axford, W. I., and C. O. Hines, A unifying theory of high-latitude geophysical phenomena and geomagnetic storms, *Can. J. Phys., 39,* 1433, 1961.

Belmont, G., F. Reberac, and L. Rezeau, Resonant amplification of magnetosheath MHD fluctuations at the magnetopause, *Geophys. Res. Lett., 22,* 295, 1995.

Cattel, C. A., F. S. Mozer, R. R. Anderson, E. W. Hones, Jr., and R. D. Sharp, ISEE observations of the plasma sheet boundary, plasma sheet, and neutral sheet, 2, Waves, *J. Geophys. Res., 91,* 5681, 1986.

Catto, P. J., M. N. Rosenbluth, and C. S. Liu, Parallel velocity shear instabilities in an inhomogeneous plasma with a sheared magnetic field, *Phys. Fluids, 16,* 1719, 1973.

D'Angelo, N., Kelvin-Helmholtz instability in a fully ionized plasma in a magnetic field, *Phys. Fluids, 8,* 1748, 1965.

Drake, J. F., J. Gerber, and R. G. Kleva, Turbulence and transport in the magnetopause current layer, *J. Geophys. Res., 99,* 11211, 1994a.

Drake, J. F., R. G. Kleva, and M. E. Mandt, Structure of thin current layers: Implications for magnetic reconnection, *Phys. Rev. Lett., 73,* 1251, 1994b.

Drake, J. F., Magnetic reconnection, a kinetic treatment, in *Physics of the Magnetopause, Geophys. Mon. 90,* Amer. Geophys. Union, Washington, D.C., 155, 1995.

Dubouloz, N., R.Pottelette, M. Malingre, G.Holmgren, and P.A.Lindqvist, Detailed analysis of broadband electrostatic noise in the dayside auroral zone, J.Geophys. Res., 96, 3565, 1991.

Ergun, R., FAST satellite observations of large-amplitude solitary structures, *Geophys. Res. Lett., 25,* in press, 1998.

Franz, J. R., Kintner, P. M., Pickett, J. S., Polar observations of coherent electric field structures, *Geophys. Res. Lett., 25,* , 1277, 1998.

Ganguly, G., M. J. Keskinen, H. Romero, R. Heelis, T. Moore, and C. Pollock, Coupling

of microprocesses and macroprocesses due to velocity shear: An application to the low-altitude ionosphere, *J. Geophys. Res., 99,* 8873, 1994.

Gary, S. P. and T. E. Eastman, The lower hybrid drift instability at the magnetopause, *J. Geophys. Res., 84,* 7378, 1979.

Gendrin, R., Magnetic turbulence and diffusion processes in the magnetopause boundary layer, *Geophys. Res. Lett., 10,* 769, 1983.

Gurnett, D.A., L.A. Frank, and R.P. Lepping, Plasma waves in the distant magnetotail, J. Geophys. Res., 81, 6059, 1976.

Gurnett, D.A., and L.A. Frank, A region of intense plasma wave turbulence on auroral field lines, J. Geophys. Res., 82, 1031, 1977.

Gurnett, D.A., and L.A. Frank, Plasma waves in the polar cusp: Observations from Hawkeye 1, J. Geophys. Res., 82, 1447, 1978.

Gurnett, D. A., R. R. Anderson, B. T. Tsurutani, E. J. Smith, G. Paschmann, G. Haerendel, S. J. Bame, and C. T. Russell, Plasma wave instabilities at the magnetopause: Observations from ISEE 1 and 2, *J. Geophys. Res., 84,* 7043, 1979.

Huba, J. D., The Kelvin-Helmholtz instability in inhomogeneous plasma, *J. Geophys. Res., 86,* 3653, 1981.

Huba, J. D., N. T. Gladd, and J. F. Drake, On the role of the lower hybrid drift instability in substorm dynamics, *J. Geophys. Res., 86,* 5881, 1981.

Kennel, C. F., and H. E. Petschek, Limit on stably trapped particle fluxes, *J. Geophys. Res., 71,* 1, 1966.

Kojima, H., H. Matsumoto, S. Chikuba, S. Horiyama, M. Ashour-Abdalla, and R. R. Anderson, Geotail waveform observations of broadband/narrowband electrostatic noise in the distant tail, J. Geophys. Res., 102, 14439, 1997.

Krall, N. A. and P. C. Liewer, Low-frequency instabilities in magnetic pulses, *Phys. Rev. A 4,* 2094, 1971.

LaBelle, J., and R. A. Treumann, Plasma Waves at the dayside magnetopause, *Space Sci. Revs., 47,* 175, 1988.

Lakhina, G. S., and A. Sen, Electromagnetic and ∇B effects on the modified two stream

instability, *Nucl. Fusion, 13*, 913, 1973.

Lakhina, G. S., Low-frequency electrostatic noise due to velocity shear instabilities in the regions of magnetospheric flow boundaries, *J. Geophys. Res., 92,* 12161, 1987.

Lakhina, G. S., Generation of low-frequency electric field fluctuations on auroral field lines, *Annales Geophysicae, 64,* 660, 1993.

Lakhina, G. S., P. K. Shukla, and L. Stenflo, Ultralow-frequency fluctuations at the magnetopause, *Geophys. Res. Lett., 20,* 2419, 1995.

Matsumoto, H., H. Kojima, T.Miyatake, Y. Omura, M.Okada, and M.Tsutsui, Electrostatic solitary waves (ESW) in the magnetotail- BEN wave forms observed by GEOTAIL, *Geophys. Res. Lett., 21*, 2915, 1994.

Mozer, F. S., R. Ergun, M. Temerin, C. Cattell, J. Dombeck, and J. Wygant, New features of time domain electric-field structures in the auroral acceleration region, *Phys. Rev. Lett., 79*, 1281, 1997.

Omura, Y., H. Matsumoto, T.Miyake, and H. Kojima, Electron beam instabilities as generation mechanism of electrostatic solitary waves in the magnetotail, J. Geophys. Res., 101, 2685, 1996.

Phillips, J. L., S. J. Bame, M. F. Thomsen, B. E. Goldstein, and E. J. Smith, Ulysses plasma observations in the Jovian magnetosheath, *J. Geophys. Res., 98,* 21,189, 1993.

Pottelette, R., M. Malingre, N. Dubouloz, B. Aparicio, R. Lundin, G. Holmgren, and G. Marklund, High-frequency waves in the cusp/cleft regions, *J. Geophys. Res., 95,* 5957, 1990.

Rezeau, L., A. Morane, S. Perraut, A. Roux, and R. Schmidt, Characterization of Alfvnic fluctuations in the magnetopause boundary layer, *J. Geophys. Res., 94,* 101, 1989.

Rome, J. A. and R. Briggs, Stability of sheared electron flow, *Phys. Fluids, 15*, 796, 1972.

Russell, C.T., R.C. Snare, J.D. Means, D. Pierce, D. Dearborn, M. Larson, G. Barr and G. Le, The GGS/POLAR magnetic fields investigation, *Space Sci. Revs., 71,* 563, 1995.

Scarf, F.L., R.W. Fredricks, I.M. Green, and C.T. Russell, Plasma waves in the dayside polar cusp, *J. Geophys. Res., 77*, 2274, 1972.

Tsurutani, B.T., E.J. Smith, R.M. Thorne, R.R. Anderson, D.A. Gurnett, G.K. Parks, C.S.

Lin, and C.T. Russell, Wave-particle interaction at the magnetopause: Contribution to the dayside aurora, *Geophys. Res. Lett., 8,* 183, 1981.

Tsurutani, B.T., and R.M. Thorne, Diffusion processes in the magnetopause boundary layer, *Geophys. Res. Lett., 22,* 663, 1982.

Tsurutani, B.T., A.L. Brinca, E.J. Smith, T. Okada, R.R. Anderson, and T.E. Eastman, A survey of ELF-VLF plasma waves at the magnetopause, *J. Geophys. Res., 94,* 1270, 1989.

Tsurutani, B.T., D. J. Southwood, E.J. Smith, and A. Balogh, A survey of low-frequency waves at Jupiter: The Ulysses encounter, *J. Geophys. Res., 98,* 21 203, 1993.

Tsurutani, B.T., and W.D. Gonzalez, The efficiency of "viscous interaction" between the solar wind and the magnetosphere during intense northward IMF events, *Geophys. Res. Lett., 22,* 663, 1995.

Tsurutani, B.T., J. K. Arballo, B.E. Goldstein, C.M. Ho, G. S. Lakhina, E.J. Smith, N. Cornilleau-Wehrlin, R. Prange, N. Lin, P. Kellogg, J.L. Phillips, A. Balogh, N. Krupp and M. Kane, Plasma wave characteristics of the Jovian magnetopause boundary layer: Relationship to the Jovian aurora?, *J. Geophys. Res., 102,* 4751, 1997.

Tsurutani, B.T., G. S. Lakhina, C.M. Ho, J. K. Arballo, C. Galvan, A. Boonsiriseth, J. S. Pickett, D. A. Gurnett, W. K. Peterson, and R. M. Thorne, Broadband plasma waves observed in the polar cap boundary layer (PCBL): POLAR, *J. Geophys. Res., 103,* in press, 1998.

Winske, D. and N. Omidi, Diffusion at the magnetopause: Hybrid simulations, *J. Geophys. Res., 100,* 11923, 1995.

Zhu, Z., P. Song, J.F. Drake, C.T. Russell, R.R. Anderson, D.A. Gurnett, K.W. Ogilvie, and R.J. Fitzenreiter, The relationship between ELF-VLF waves and magnetic shear at the dayside magnetopause, *Geophys. Res., Lett., 23,* 773, 1996.

G.S. Lakhina and B.T. Tsurutani, Jet Propulsion Laboratory, California Institute of Technology, 4800 Oak Grove Drive, Pasadena, California 91109. (e-mail: lakhina@jplsp.jpl.nasa.gov; btsurutani@jplsp.jpl.nasa.gov)

Received February 4, 1998

[1] Permanent Address: Indian Institute of Geomagnetism, Colaba, Bombay 400005, India.

Submitted to *Journal of Geophysical Research*, 1998.

Figure 1. Variation of normalized growth rate, γ/ω_{ci}, (upper panel) and normalized real frequency, ω_r/ω_{ci},(lower panel) versus velocity shear $S = \frac{1}{\omega_{ce}}\frac{dV_0}{dx}$ for the electrostatic ($R = \omega_{pe}^2/c^2k^2 = 0$) current convective instability for the case of cold plasma with $\omega_{pe}/\omega_{ce} = 10$, and $V_0 = 0$. The curves 1 and 2 are for k_z/k_y = -0.1 and -0.005, respectively, and the instability is purely growing (i.e., $\omega_r = 0$). The curves 3, 4 and 5 are for k_z/k_y = -0.1 and $(\kappa_n - \kappa_B)/k_y$ = 0.05, 0.11, and 0.2, respectively.

Figure 2. Variation of normalized growth rate, γ/ω_{ci}, (upper panel) and normalized real frequency, ω_r/ω_{ci},(lower panel) versus velocity shear $S = \frac{1}{\omega_{ce}}\frac{dV_0}{dx}$ for the current convective instability for the case of cold plasma with $\omega_{pe}/\omega_{ce} = 10$, $V_0 = 0$, and k_z/k_y = -0.1. The curves 1, 2 and 3 are for $(\kappa_n - \kappa_B)/k_y$ =0.0, and $R = \omega_{pe}^2/c^2k^2$ = 0.0, 1.0, and 5.0, respectively. The curves 4, and 5 are for $(\kappa_n - \kappa_B)/k_y$ = 0.1, and R = 1.0, and 5.0, respectively.

Figure 3. Variation of normalized growth rate, γ/ω_{ci}, (upper panel) and normalized real frequency, ω_r/ω_{ci}, (lower panel) versus normalized drift velocity $\frac{k_y V_d}{\omega_{ci}}$ for the lower hybrid instability for the case of cold plasma with $\omega_{pe}/\omega_{ce} = 10$, $V_0 = 0$, and k_z/k_y = -0.1 (except for curve 5). The curve 1, 2, and 3 are for $(\kappa_n - \kappa_B)/k_y = 0.0$, $S = 0$, and $R = \omega_{pe}^2/c^2k^2$ = 0.0, 1.0, and 5, respectively. For the cureves 4 and 5, $R = 0$, $(\kappa_n - \kappa_B)/k_y$ = 0.0, S = 0.04 and k_z/k_y = -0.1 and 0.1 respectively. The curves 6, and 7 are for R = 0, $S = 0$ and $(\kappa_n - \kappa_B)/k_y$ = 0.1, and 0.2, respectively.

Figure 4. Variation of normalized growth rate, γ/ω_{ci}, (upper panel) and normalized real frequency, ω_r/ω_{ci},(lower panel) versus normalized wavenumber $a = k_y V_{ti}/\omega_{ci}$ for the electrostatic lower hybrid drift instability for the case of hot plasma with $S = 0.0$, $V_0 = 0$, $\beta_i = 0.0$, and $\kappa_B/k_y = 0.0$. For the curves 1,2 and 3, $\omega_{pe}/\omega_{ce} = 10.0$, $T_e/T_i = 1.0$, $\kappa_n/k_y = 0.1$, and k_z/k_y = -0.01, -0.1 and -0.2, respectively . For the curve 4, k_z/k_y = -0.1 and $\kappa_n/k_y = 0.2$ (other parameters are the same as for the curves 1-3). The curves 5 and 6 are for k_z/k_y = -0.01, $\kappa_n/k_y = 0.1$, $\omega_{pe}/\omega_{ce} = 1.0$, and $T_e/T_i = 1.0$ and 3.0, respectively. The sign of the parameter k_z/k_y does not affect the growth rates and the real frequencies.

Figure 5. Variation of normalized growth rate, γ/ω_{ci}, (upper panel) and normalized real frequency, ω_r/ω_{ci}, (lower panel) versus normalized wave number number $a = k_y V_{ti}/\omega_{ci}$ for the coupled current convective and lower hybrid drift instability for the case of hot plasma with $S = 0.1$, $\omega_{pe}/\omega_{ce} = 3.0$, V_0=0, $\kappa_n/k_y = 0.01$, and k_z/k_y = -0.01. The curves 1, 2 and 3 are for $T_e/T_i = 1.0$, and $\beta_i = 0.0$, 0.1, and 0.2, respectively. The curve 4 is for $\beta_i = 0.2$ and $T_e/T_i = 0.2$. The values for the magnetic field gradient used here and in Figure 6 are obtained from the relation $\kappa_B = -\beta_i(1 + T_e/T_i)\kappa_n/2$.

Figure 6. Variation of normalized growth rate, γ/ω_{ci}, (upper panel) and normalized real frequency, ω_r/ω_{ci}, (lower panel) versus normalized wavenumber number $a = k_y V_{ti}/\omega_{ci}$ for the coupled lower hybrid drift and current convective instability for the case of hot plasma with $\omega_{pe}/\omega_{ce} = 10.0$, V_0=0, and $\kappa_n/k_y = 0.1$. The curves 1, 2, and 3 are for $\beta_i = 0.0$, k_z/k_y = -0.1 and $S = \frac{1}{\omega_{ce}}\frac{dV_0}{dx} = 0.0$, 0.05, and 0.1, respectively. The curv 4 is for β_i = 0.0, $S = 0.1$, and $k_z/k_y = 0.1$. The curves 4 and 5 are for $S = 0.1$, k_z/k_y = -0.1 and β_i = 0.05 and 0.2, respectively.

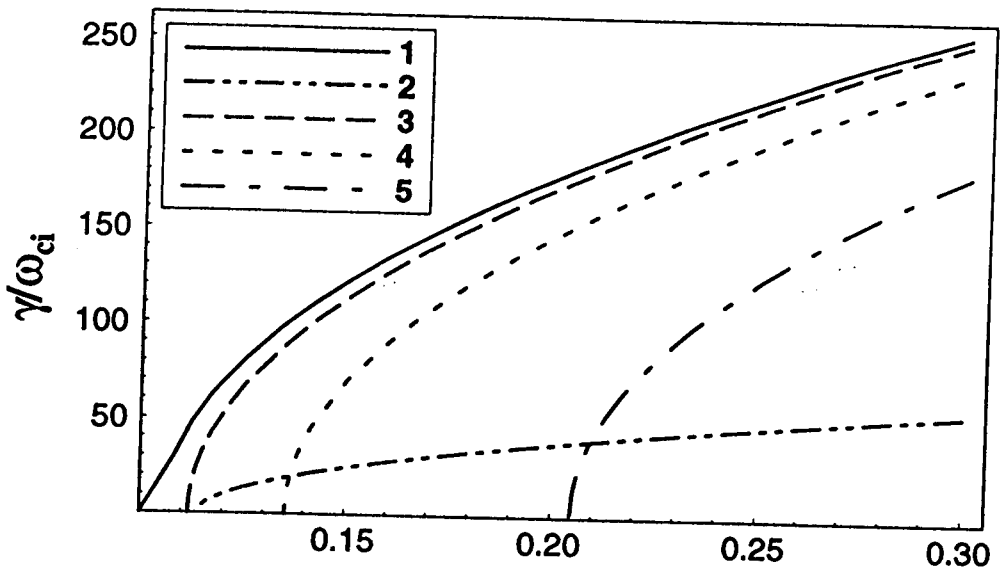
250
200
150
100
50
γ/ω_{ci}
1
2
3
4
5
0.15
0.20
0.25
0.30
s

a)

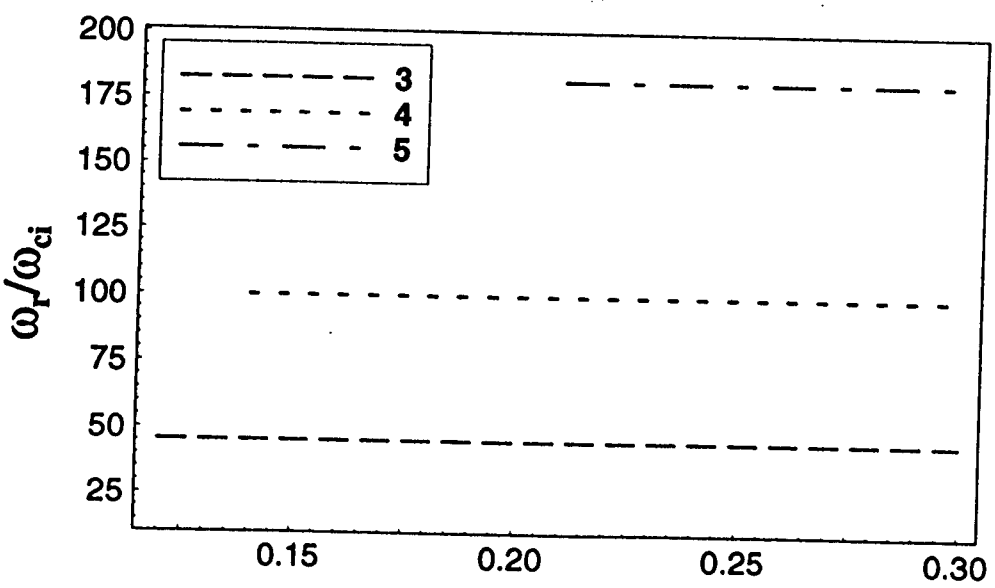
200
175
150
125
100
75
50
25
ω_r/ω_{ci}
3
4
5
0.15
0.20
0.25
0.30
s

b)

Fig. 1

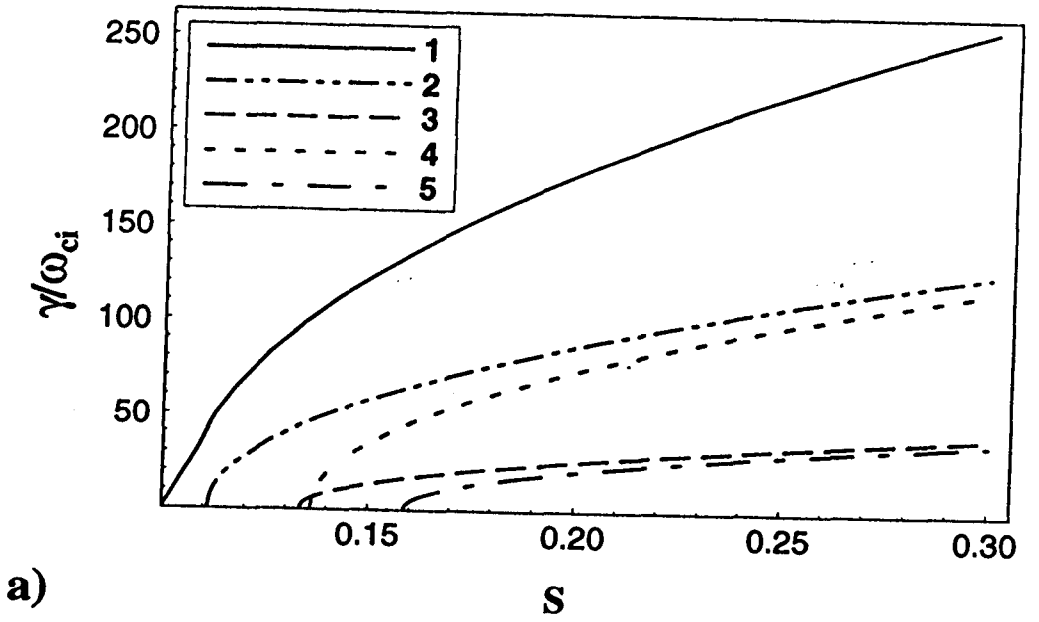
250
200
150
100
50
γ/ω_ci
1
2
3
4
5
0.15
0.20
0.25
0.30
s

a)

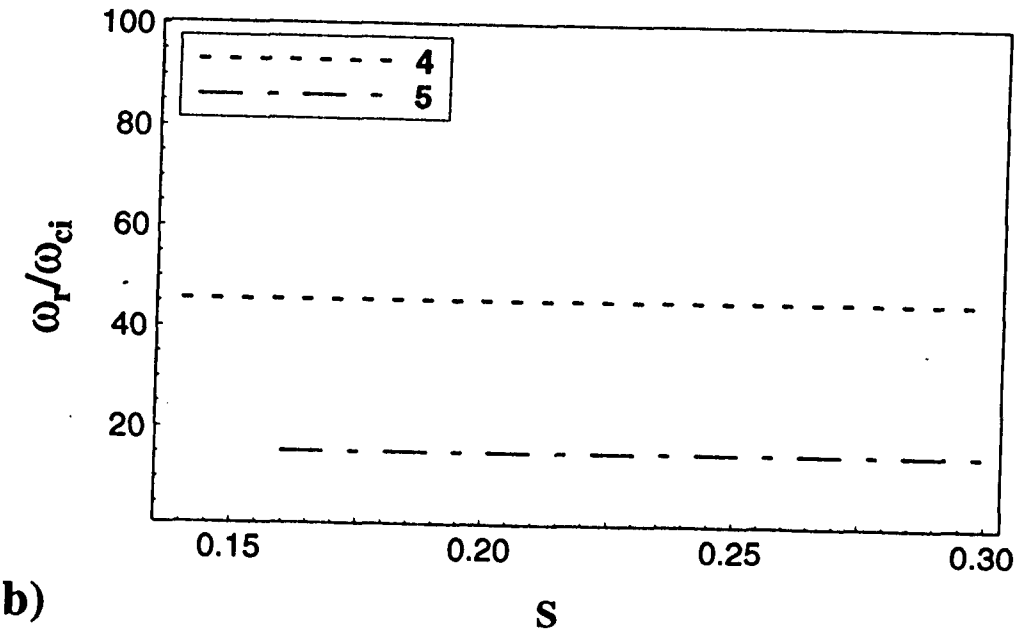
100
80
60
40
20
ω_r/ω_ci
4
5
0.15
0.20
0.25
0.30
s

b)

Fig. 2

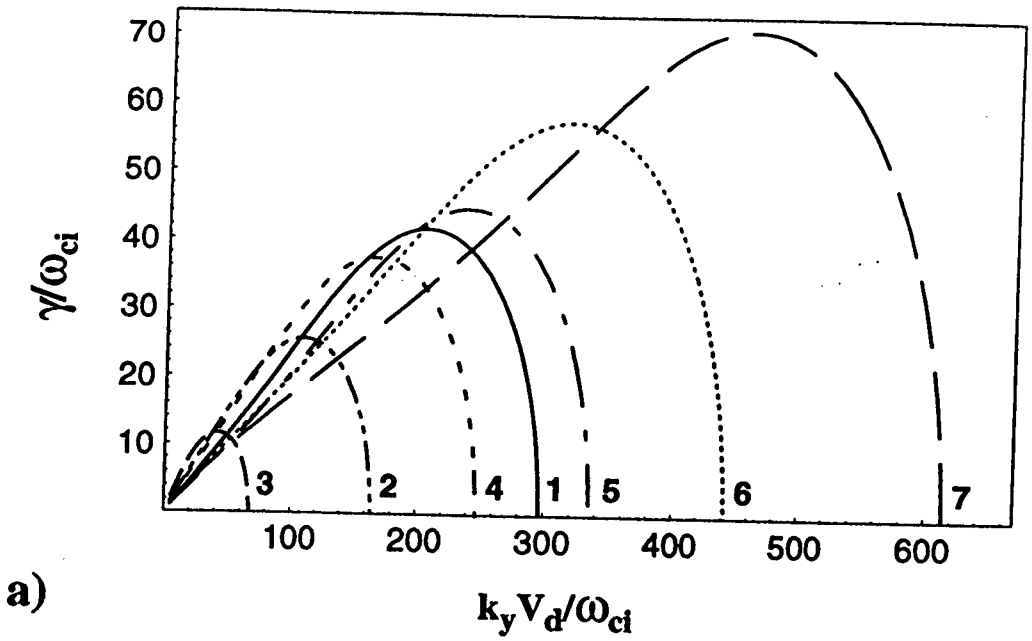
70
60
50
40
30
20
10
γ/ω_ci
3
2
4
1
5
6
7
100
200
300
400
500
600
k_y V_d/ω_ci

a)

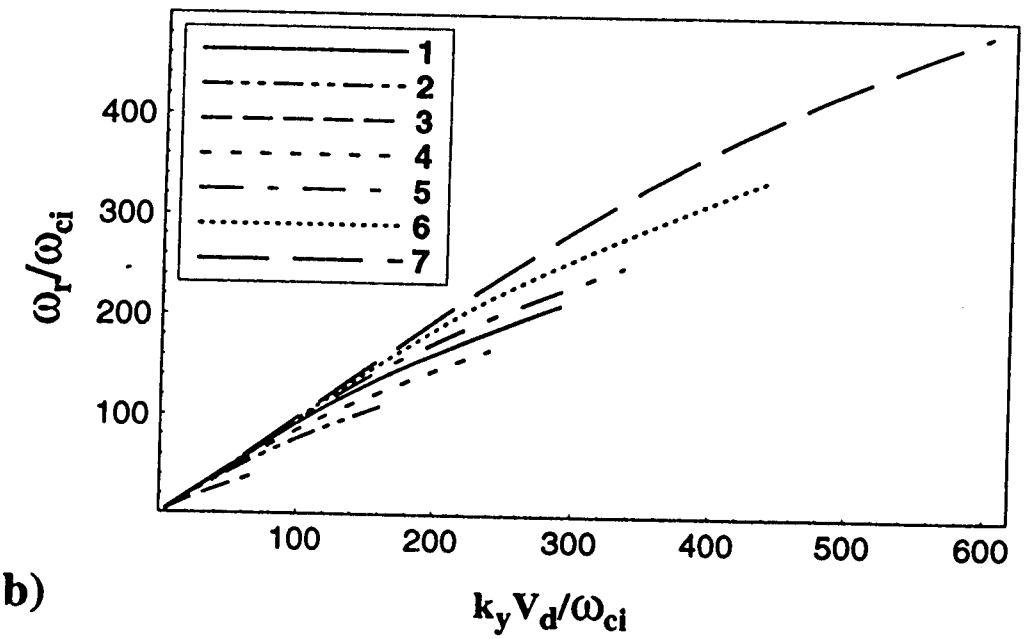
1
2
3
4
5
6
7
400
300
200
100
ω_r/ω_ci
100
200
300
400
500
600
k_y V_d/ω_ci

b)

Fig. 3

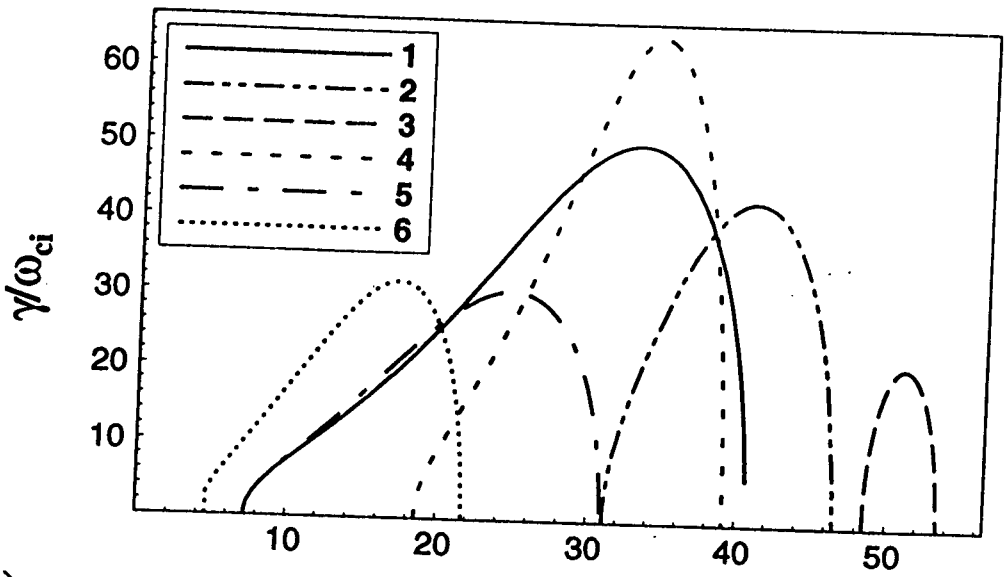
1
2
3
4
5
6
60
50
40
30
20
10
10
20
30
40
50
γ/ω_ci
a

a)

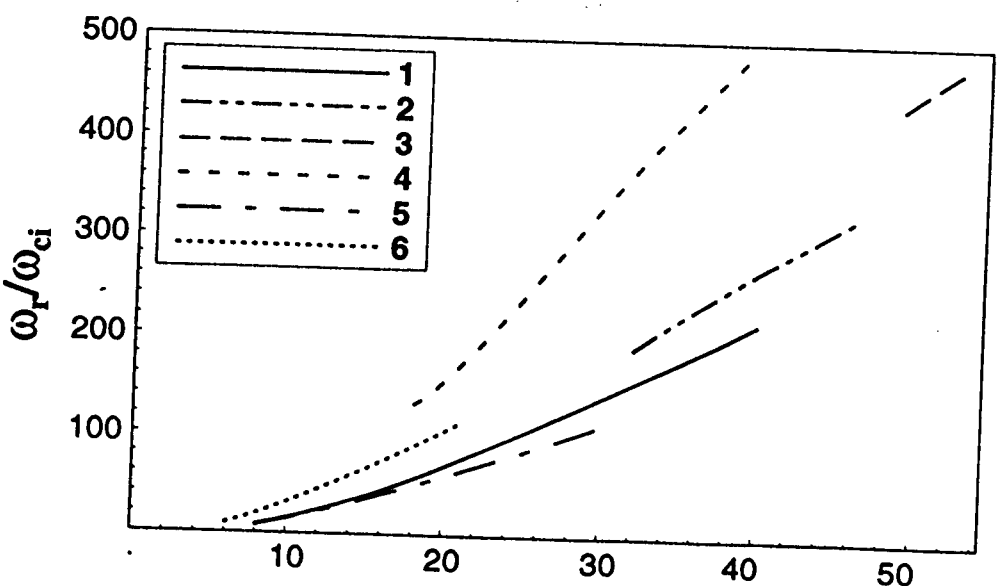
1
2
3
4
5
6
500
400
300
200
100
10
20
30
40
50
ω_r/ω_ci
a

b)

Fig. 4

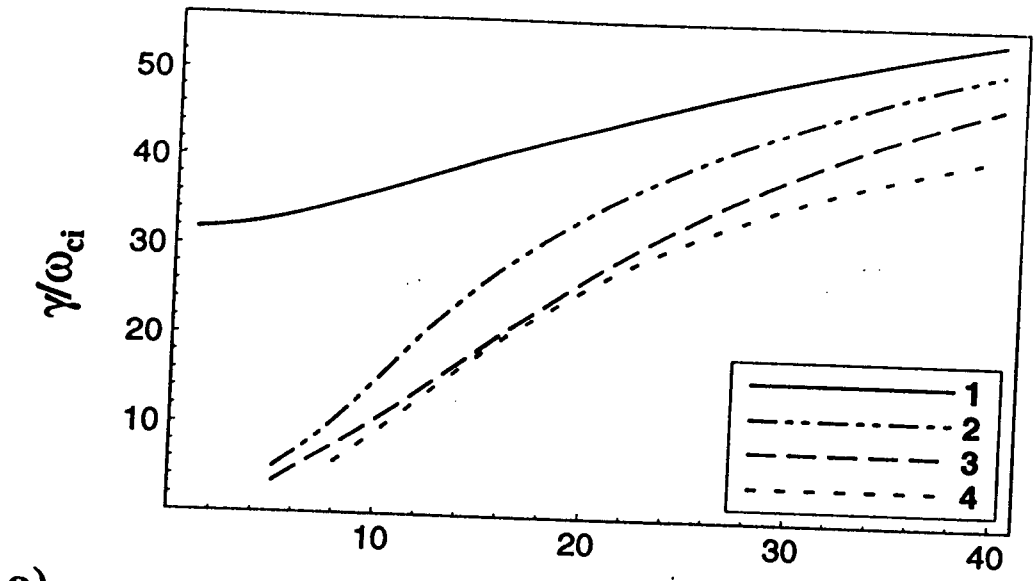

a)

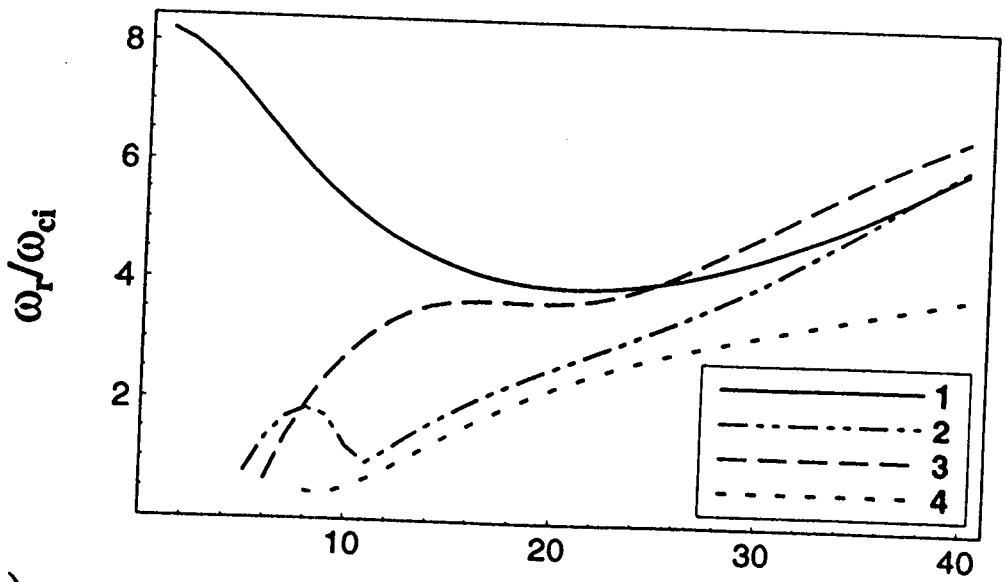

b)

Fig. 5

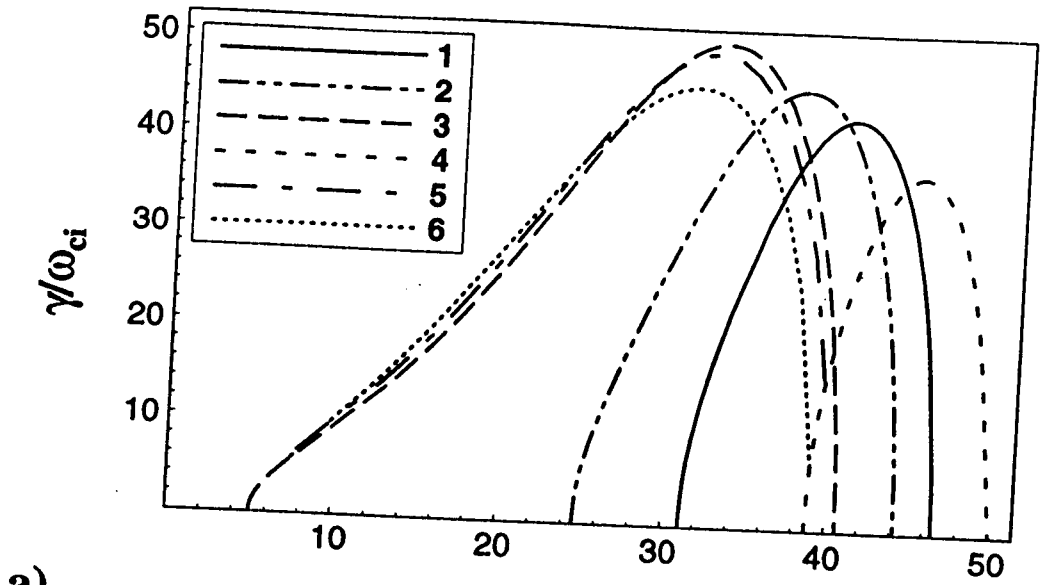
50
40
30
20
10
γ/ω_ci
1
2
3
4
5
6
10
20
30
40
50
a

a)

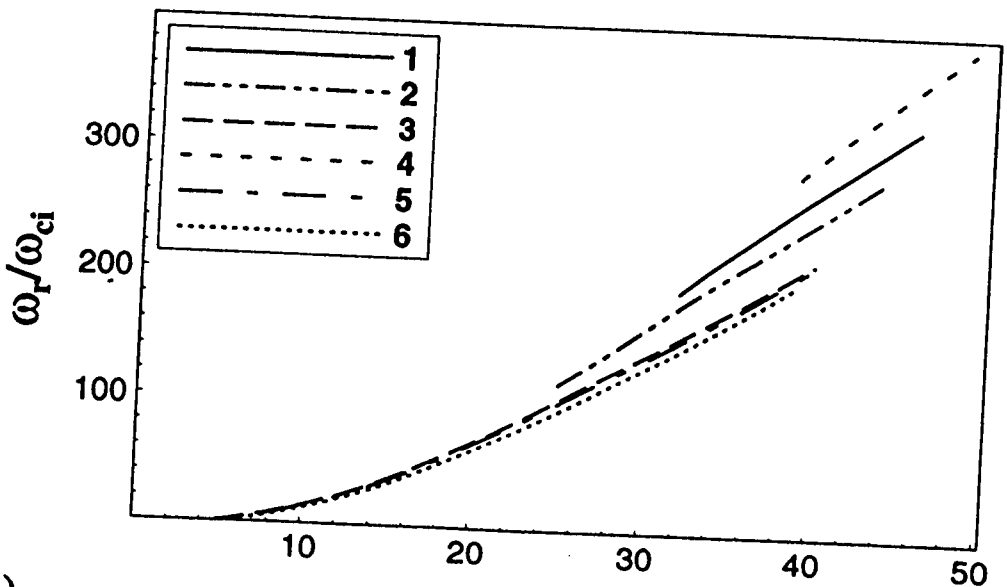
300
200
100
ω_r/ω_ci
1
2
3
4
5
6
10
20
30
40
50
a

b)

Fig. 6

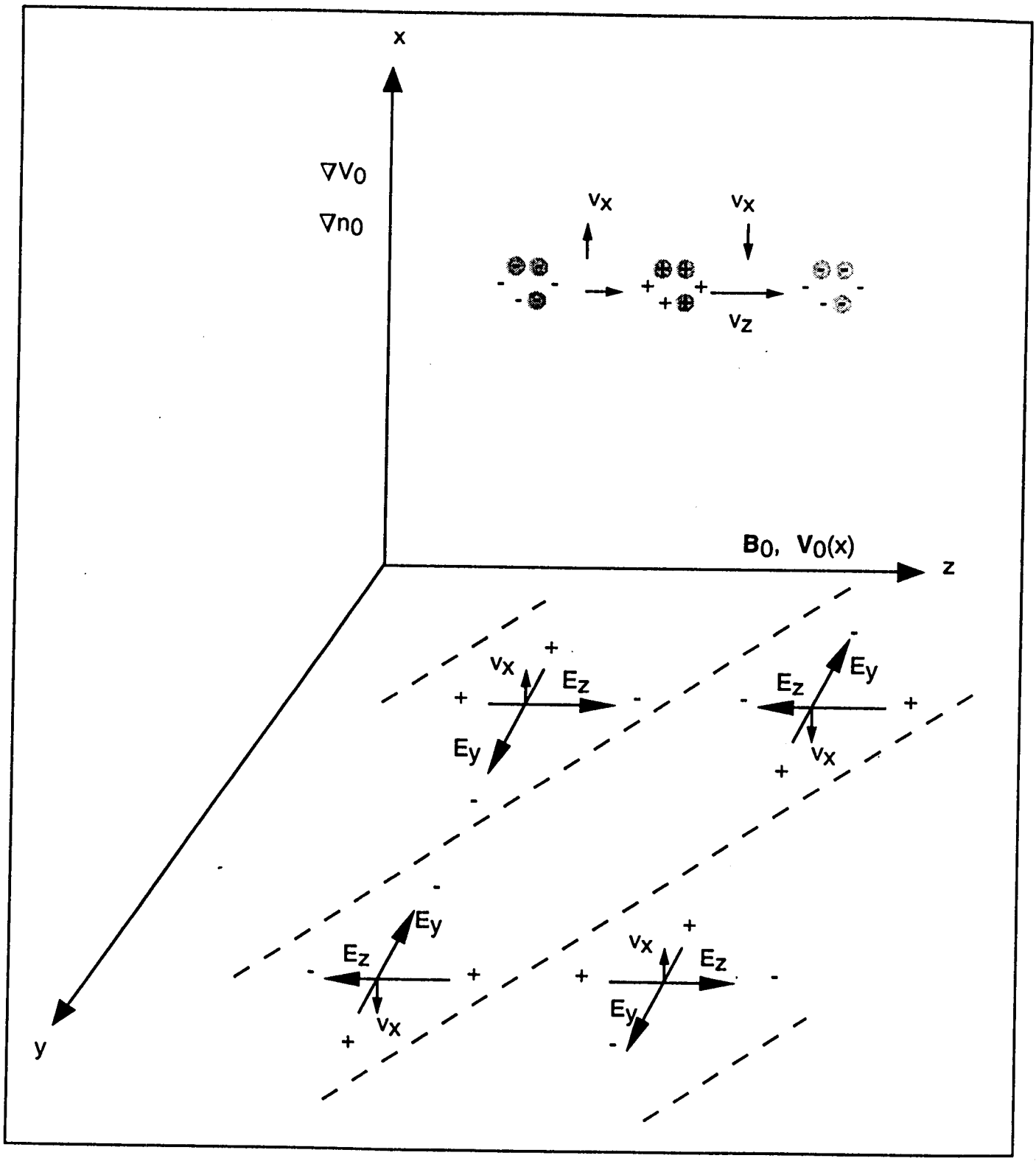

Figure 7